NUMERICAL AND EXPERIMENTAL INVESTIGATION OF AN EMBARKED VIBRO-IMPACT SYSTEM

Romulo R. Aguiar, romulo@aluno.puc-rio.br
Hans I. Weber, hans@puc-rio.br
Mechanical Engineering Department, PUC-Rio
Rua Maquês de São Vicente, 229, Gávea
22453-900, Rio de Janeiro - RJ - Brazil

Abstract. There are technical applications where a main part of the mechanical system is subjected to a regular vibration pattern. An example is the oil well drilling with tricone bits on hard material, since in a regular condition of the contact surface, it is imposed a longitudinal vibration on the drilling structure. It is possible to use a part of this energy to resonate some sort of a hammer, which is a substructure of the main system, that generates impacts. The stress wave created by such impacts may be useful to release the system from a stick condition of stick-slip phenomena or to help in the crack propagation of the material that is being cut. In oil well drilling, the task to develop an internal hammer in the bottom hole assembly that impacts during the drilling process is still a suggestion to be implemented. This work presents basic studies for this development. The purpose of this work is the numerical/ experimental investigation of the impact force behavior in a vibro-impact system, where such hammer is embarked on a cart that moves by a prescribed displacement. By changing the hammer characteristics and the impact gap, it is possible to investigate the impact force behavior under different excitation frequencies. The experimental data will be used to validate the mathematical model, where the system behavior is investigated in more detail, as well as a nonlinear analysis (bifurcation diagrams, Poincaré maps and Peterka map) is performed, showing the rich response of the system, such as dynamical jumps, bifurcations and chaos.

Keywords: nonlinear dynamics, vibro-impact system, contact dynamics

1. INTRODUCTION

During oil well drilling, it is well known that undesirable vibration leads to failure of drill pipes, intensive bit wear and increase of overall cost. Drillstring vibration is complex in nature and couples axial, bending and torsional vibration (Dykstra, 1996). To eliminate the negative effects of the vibration, improvements are constantly brought in, through new concepts of drilling and new designs. These new approaches have to consider the efficient use of energy as an important factor, bringing an increase in bit life, in rate of penetration and reduced cost in hard rock drilling.

In the field there are two main drilling techniques. Conventional rotary drilling is the most economical and typically drills holes of up to 850 mm in diameter. In rotary drilling, cutting of rock is achieved by a rotating drill bit under load. In the other hand, percussive drilling fragments rock formations by means of blows, which occur only for a fraction of time. This method relies entirely on crack propagation and brittleness of the formation. Percussion drilling is preferable on very hard sedimentary rocks, due to low bit wear and fast penetration, but this method cannot produce the same rate of penetration when drilling at greater depth.

In this context, optimum productivity is possible by combining advantages of both existing drilling techniques: rotary and percussive drilling. In conventional rotary drilling, the energy applied in the system (oil well drillstring) comes from the rotary table, located at the top of the drillstring. Such energy, supplied to drill the oil well, ends up being wasted by vibration (axial, torsional and bending), friction with borehole walls and heat. If part of the energy wasted in vibration could be reinserted into the drilling process, the rate of penetration (ROP) can be increased. The idea is to use the percussive drilling into rotary drilling to reinsert this energy. In this way, such technique for oil well drilling is being called **Resonance Hammer Drilling** (Detournay, 2004), Fig.1*(left)*.

The use of the already existent vibrations in the drillstring, in fact the axial vibration due to the cutting process, to generate a harmonic load on the bit and an excitation in a steel mass (hammer) which will cause impacts is the motivation of this work. The concept of this hybrid technique is to reinsert the energy wasted on axial vibration, back into the drilling process, with the use of impacts. The stress waves created by such impacts may be useful to release the system from a stick condition of stick-slip phenomena, as well as generating cracks on the rock formation, increasing ROP.

Several investigations were performed in the past. The first one is presented by Franca and Weber (2004). In this work, a model for the longitudinal behavior of the bit-rock with a vibro-impact system was investigated. As conclusion, the behavior of period-1 with one impact per cycle is always the best condition of penetration, increasing the ROP. A second investigation was presented by Aguiar and Weber (2008, 2009). In these works, a new mechanism to enhance the drill string rate of penetration is experimentally investigated. Such hammer, in order to create impact forces from the axial vibration of the drill string, was called "RIMD" (**R**esonant **IM**pact **D**evice). It is presented a test rig simulating the RIMD performance and the drillstring behavior influence on the RIMD.
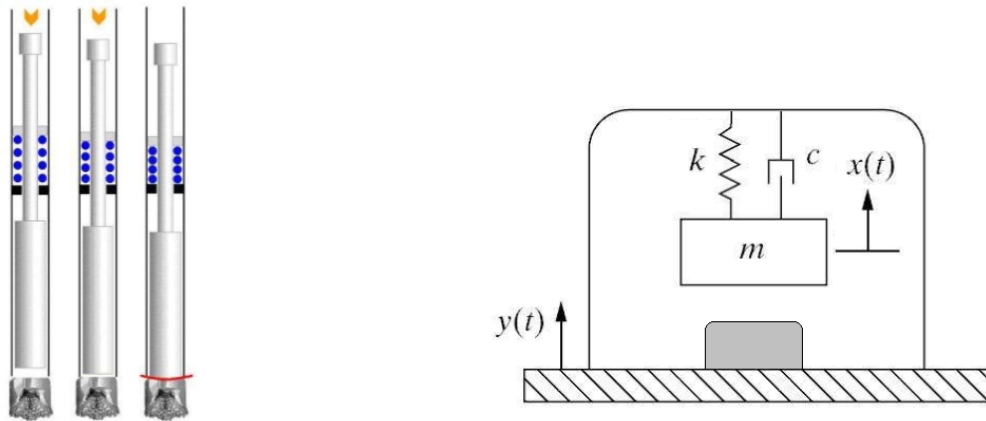
Figure 1. Resonance hammer drilling technique *(left)*; Vibro-impact system *(right)*.

1.1 Objectives

This present work is focused on the mathematical modeling of the experimental test rig presented in Aguiar and Weber, 2008. In this case, the experimental data will be used to validate a mathematical model, where the system behavior is investigated in more detail, as well as a nonlinear analysis (bifurcation diagrams, Poincaré maps and Peterka map) is performed, showing the rich response of the system, such as dynamical jumps, bifurcations and chaos. Such mathematical model will allow further investigations on this subject providing different ways to other RIMD possible constructions.

First, a study is driven in order to identify which impact model better reproduces the experimental data. After all parameters are identified, the simulations are performed and a comparison between numerical simulations and experimental data is carried. Finally, the system is analyzed in terms of nonlinear tools.

2. EXPERIMENTAL APPARATUS, METHODOLOGY AND RESULTS

The experimental apparatus, shown in Fig.2, was designed to represent the drillstring axial behavior and its influence over the impact device (RIMD). The experiment is composed by two systems, both moving from the equilibrium position over the horizontal direction.

The first system englobes the low friction rail (steel); the cart (aluminum), which can slide along the horizontal axis over the low friction rail assembly; and the excitation source, an AC motor attached to the cart through a pin that can slide over a groove machined on a nylon plate fixed on the cart. Once the pin hole is drilled off-centered on the rotating disk, the rotational movement of the motor is turned into a sinusoidal cart movement. Actual excitation source allows to develop higher amplitudes and also avoids the influence of the generated impact forces on the base excitation (more suitable with real operation). Such advantages would not be achievable with a electromagnetic shaker, an experience gained from previous experimental set ups (Aguiar and Weber, 2008).

The second system is composed by the RIMD, a mass-spring embarked inside the cart. RIMD mass is composed by one of the aluminum couplings that holds the springs and by the impact device (steel). RIMD can be supported by either a series of 8 nylon wires or two clamped-clamped bending beams. In this work the focus is on the mathematical modeling of the RIMD supported by wires, therefore just the experimental results for this configuration will be shown. As shown in Fig.2, eight nylon wires are used, in order to assure that RIMD moves only in the axial direction. Also, the wires are hung into the cart structure in angle (around 30 degrees with vertical axis), so the RIMD rotation after impact is eliminated or minimized.

In order to change the gap between the RIMD and the cart, the impact device is composed by a long screw and a knurled nut, where the gap can be measured using calibrated shims. The test rig is instrumented with one accelerometer attached to the back of the RIMD (Endevco 751-10 SN AC70); one piezoelectric force sensor (PCB 208C03), fixed on the cart and located in front of the RIMD impact device; and two laser displacement sensors, both located on the side of the cart. One of the laser displacement sensors is measuring the cart displacement (optoNCDT 1607-20) and the second one measures the RIMD displacement (optoNCDT 1607-100). In order to measure the RIMD displacement, a vertical groove is machined on the cart wall so the beam from the second laser displacement sensor is capable to reach the hammer. The four output parameters are acquired in two different oscilloscopes, in order to better capture the impact phenomenon. The impact force and the RIMD acceleration signals are acquired into one oscilloscope, with a time scale of milliseconds (sometimes microseconds), while the displacement signals are acquired in another oscilloscope, with a time scale of seconds. Impact force and acceleration signals are triggered in order to capture the exact instant of impact.

The input parameter is the excitation frequency from the AC motor, where the pin is drilled 1 mm off-centered. The
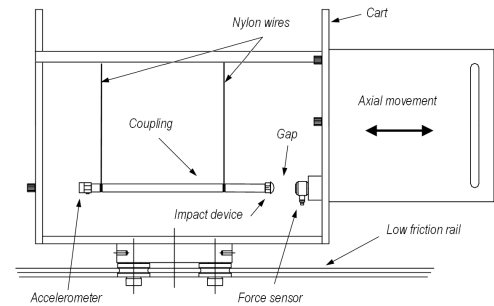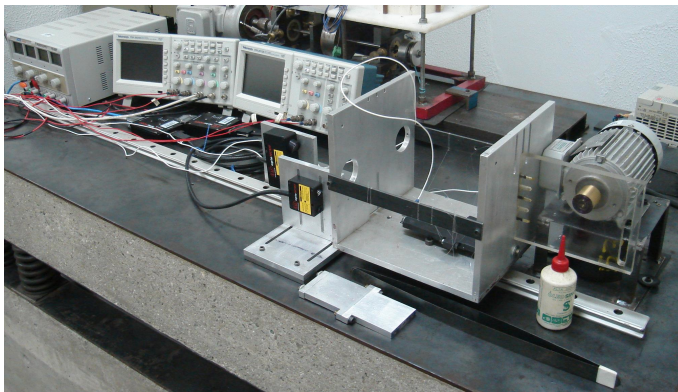
Figure 2. Test rig photo and experiment sketch.

experiment parameter is the impact gap. The outputs are: the acceleration signal from the accelerometer mounted on the top of the RIMD; the impact force applied by the RIMD; the cart displacement, measured through a laser displacement sensor and the RIMD displacement, measured also using a laser displacement sensor. Both displacement measures are taken outside the cart, therefore are in an inertial frame of reference. As it will be discussed later, once generalized coordinate in the equation of motion is embarked on the cart, some transformations are necessary in order to compare the experimental data with simulation results.

The methodology applied is to observe the behavior of the impact system as the gap is varied. In this case, the RIMD stiffness is kept constant while three values of gap were chosen, 0.0 mm, 1.0 mm and 2.4 mm. System parameters are identified for the case without impact and a study with impact is carried out as the gap is modified. The excitation frequency from the AC motor is changed in order to sweep the range of frequencies.

2.1 Experimental results

In the case of no impact, the RIMD has the exact behavior of a one-degree-of-freedom system excited by an harmonic load (in this case, a base excitation), even showing the *beat* phenomenon. Since such system is well known and widely described in literature, no further comments will be addressed.

As already noted in previous works (Aguiar and Weber, 2008, 2009), the RIMD impact force behavior can be split into frequency bands, showing similar characteristics in each frequency band regardless of which gap is investigated. In the very first excitation frequencies (less than 2.5 Hz), the cart movement is so slow that the RIMD basically follows the prescribed excitation, generating two or three impacts per excitation cycle with extremely low impact forces. In frequency band **A**, the impact force presents a period-1 stable behavior, with the impact force peak increasing as the excitation frequency increases, reaching its highest value at 3.75 Hz (82.4 N) and after this frequency the impact force decreases while the frequency is raised. Figure 3 shows the impact force, RIMD acceleration and both cart and RIMD displacements for the maximum impact force of frequency band **A**.
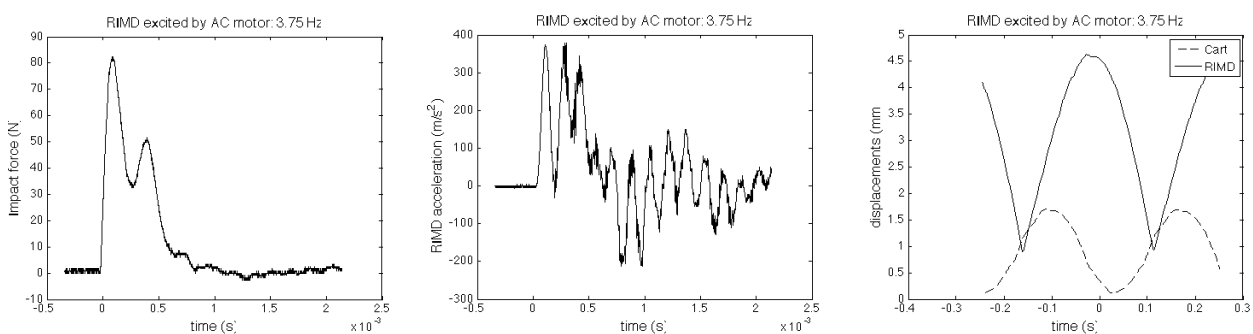
Figure 3. RIMD impact force behavior. Gap 0.0 mm. Frequency band **A**, $\Omega = 3.75 Hz$. *left*) Impact force over time; *center*) RIMD acceleration over time; *right*) displacements (cart and RIMD)

The impact force transducer captures well the first impulse transferred by the hammer, until the maximum around 80N. In a second moment, in this micro scale analysis, the impacted structure will give some impulse back to the hammer, and will react according to an own dynamics originating a second peak around 50N. The accelerometer measures the hammer dynamics, since it is fixed to the opposite side of the impact device, see Fig. 3. The fact that exists some contact dynamics is strengthen by the acceleration chart, once there are unexpected oscillations after the impact, which may lead to the hypothesis that RIMD has an axial vibration behavior that is relevant to the impact process. At the end of frequency

band **A**, systems presents a bifurcation in the impact force behavior, characterized by a period-1 impact with low peaks an alternate impact magnitudes, as shown in Fig. 4.
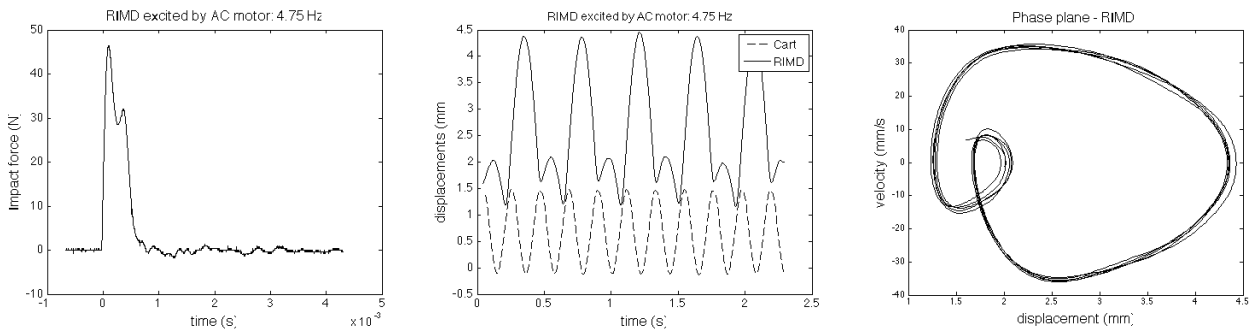
Figure 4. RIMD impact force behavior. Gap 0.0 mm. Bifurcation, $\Omega = 4.75Hz$. *left*) Impact force over time; *center*) RIMD and cart displacements; *right*) RIMD phase plane

Frequency band **B** presents a similar curve to frequency band **A**, however the impact force occurs every two excitation cycles, with the impact force peak raising as the frequency increases, reaching its highest value at 7.25Hz (120N). After reaching such maximum, the impact force peak decreases as the frequency increases. The excitation frequency where the maximum impact force occurs on frequency band **B** is exactly two times the excitation frequency where the maximum impact force occurs on frequency band **A**. Charts showing the output parameters for the maximum impact force on frequency band **B** are shown in Fig. 5. Right after frequency band **B** the system shows another transitory behavior, with similar behavior observed in the previous transitory band.
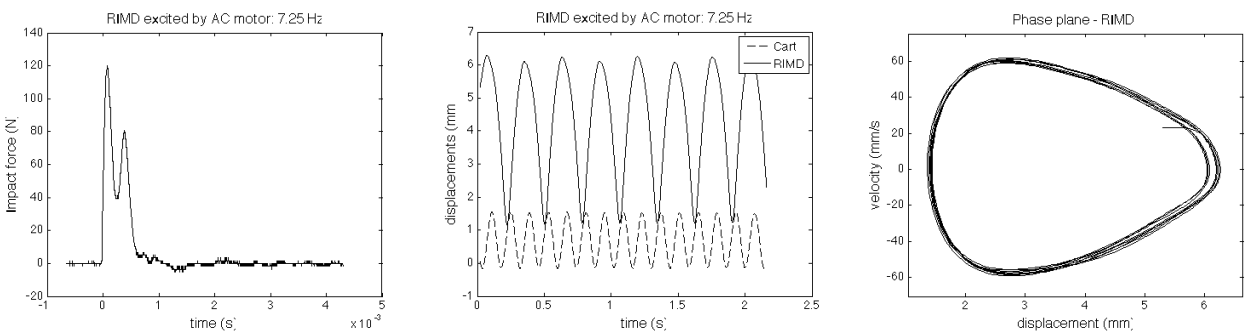
Figure 5. RIMD impact force behavior. Gap 0.0 mm. Frequency band **B**, $\Omega = 7.25Hz$. *left*) Impact force over time; *center*) RIMD acceleration over time; *right*) displacements (cart and RIMD)

With such experimental data it is possible to analyze the system behavior in the frequency domain. In order to, a computational routine is created so as to determine the F_i (impact force peak). For F_i, the maximum value is extracted. Once impact force results do not change the peak value in each excitation frequency, except for the transitory bands, this routine seems to be quite effective, specially around the maximum impact force peaks. Finally, in order to generate a non-dimensional chart so as to compare it to the answers in the other configurations, the force ratio F_i/mg is used (mg is weight of RIMD), as well as the excitation frequency is divided by the system natural frequency without impact, experimentally identified using modal analysis. The charts showing the system behavior for each chosen gap are shown in Fig. 6.

At this point is important to remind that, although the maximum impact force on frequency band **B** is higher than frequency band **A**, in frequency band **B** impacts occur every two cycles and also that energy inserted into the system increases with the square of the excitation frequency. Once displacement is prescribed, the magnitude of the excitation force F_{exc} is equal to $m_{tot} A_0 \Omega^2$, where m_{tot} is the total mass (cart and RIMD inertias), A_0 is the displacement amplitude and Ω is the excitation frequency.

Using a concept from the linear theory to describe a nonlinear behavior, it is considered *impact resonance* the excitation frequency where the maximum impact force is achieved. Once RIMD displacement is limited by a gap, an interesting phenomenon occurs. The presence of the impacts significantly alters the value of the impact resonance, if compared to the system resonance, as it can be observed in Tab. 1. This alteration of resonance in the presence of impacts was already studied (Mattos and Weber, 1994) and expected.
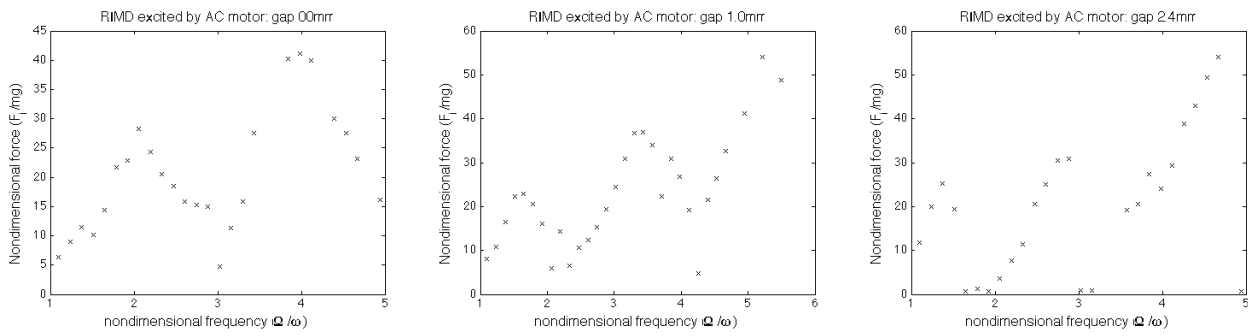
Figure 6. RIMD impact force behavior. Frequency domain response, maximum non-dimensional force, F_i/mg. *left*) Gap 0.0 mm. *center*) Gap 1.0 mm. *right*) Gap 2.4 mm.

Table 1. Impact resonance frequencies (experimental).

Frequency band	A (1 impact/ cycle)	B (1 impact/ 2 cycles)
gap 0.0mm	$3.75 Hz$	$7.25 Hz$
gap 1.0mm	$3.00 Hz$	$6.25 Hz$
gap 2.4mm	$2.50 Hz$	$5.25 Hz$
System natural frequency (gap $\to \infty$)	$1.82 Hz$	

3. MATHEMATICAL MODELING AND NUMERICAL/ EXPERIMENT COMPARISON

3.1 Impact model for RIMD modeling

In order to adopt an impact model capable of describing the real impact observed during the experiments in this work, some hypothesis are adopted:

1. impact is central and collinear, i.e., the center of mass of both bodies relies on the impact line;

2. impact velocity is along the impact line;

3. contact tangential force is always zero, once impact is collinear and there is no impact velocity component in tangential axis.

In this way, four impact models where used in other to describe the RIMD impact, all using continuous analysis. Such approach is based on the fact that the interaction forces act in a continuous manner during the impact. Thus, the analysis may be performed in the usual way, by simply adding the contact forces to the equations of motion during their action period. This allows a better description of the real behavior of the system. More importantly, this approach is naturally suitable for contact modeling and complex contact scenarios involving multiple contacts and bodies (Gilardi and Shaft, 2002). The four impact models used where: Hertz's impact model, spring-dashpot model, Hunt and Crossley and Lankarani, all listed in Eq. 1.

$$\text{Hertz's model}: F_i = k_i \delta^{n_i} \qquad\qquad \text{Spring} - \text{dashpot}: F_i = k_i \delta + c_i \dot{\delta}$$

$$\text{Hunt and Crossley}: F_i = k_i \delta^{n_i} + c_i \delta^{n_i} \dot{\delta} \qquad\qquad \text{Lankarani}: F_i = k_i \delta^n \left[1 + \frac{3(1-e^2)}{4} \frac{\dot{\delta}}{\delta^{(-)}} \right] \qquad (1)$$

Hert's law of impact is a nonlinear model, but limited to impacts with elastic deformation, and in its original form does not include damping. With this model, the contact process can be pictured as two rigid bodies interacting via a nonlinear spring along the line of impact.

In the spring-dashpot model, impact is schematically represented with a linear damper (dashpot) for the dissipation of energy in parallel with a linear spring for the elastic behavior. Although such model is not physically realistic, its simplicity has made it a popular choice. It provides a reasonable method for capturing the energy dissipation associated with the normal forces without explicitly considering plastic deformation issues.

To overcome the problems of the spring-dashpot model and to retain the advantages of the Hertz's model, an alternative model for energy dissipation was introduced by Hunt and Crossley (1968), introducing a nonlinear (hysteresis) damping term.

Finally, Lankarani and Nikravesh (1994) developed a contact force model with hysteresis damping for impact in multibody systems. This model uses the general trend of the Hertz contact law, in which a hysteresis damping function was incorporated in the model that represents the energy dissipated during the impact.

In order to better identify the impact parameter, a second impact body (hammer) was built. The idea is to remove the influence of the axial vibration behavior while characterizing and identifying the impact force. The new hammer is made of steel (original is made of aluminum). Using the same screw with knurled nut and impact force sensor, impact conditions will be reproducible, once impact depends only on the materials and geometries involved during contact. To identify the impact force parameters, a simpler experiment is performed, where a well known initial condition is imposed and the experimental response is compared to the simulation. In this case all impact models listed were compared to the experimental data. A optimization procedure is performed, in order to minimize the difference in the impact force peak as well as the impulse between experimental data and numerical simulations. Although the spring-dashpot model is not capable of reproducing the real impact force profile over time, due to the jump caused by the damping force, this model generated the best results. Impact parameters for this model are listed in Tab. 2.

Table 2. Impact parameters - spring-dashpot model.

Parameter	Value	Unit
Impact stiffness, k_i	$5.5 \cdot 10^6$	N/m
Impact damping, c_i	$1.2 \cdot 10^3$	Ns/m

The mathematical modeling for the first test rig, i.e., RIMD supported by nylon wires, is presented below. As θ the generalized coordinate, RIMD can be modeled as a single pendulum embarked in a prescribed movement, where the impact surface is also moving with the system, once the impacts are embarked, as shown in Fig. 7.
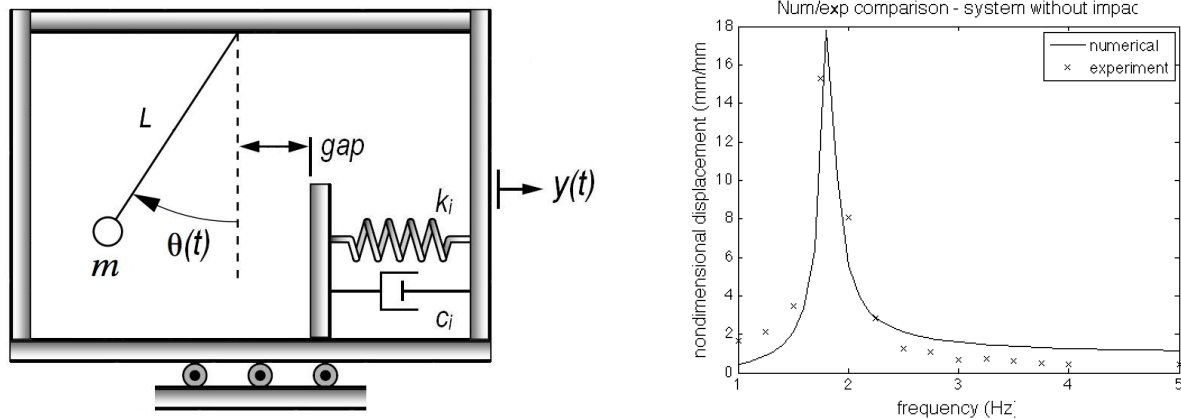
Figure 7. Model of RIMD supported by wires, physical representation. RIMD wires, no impact. Numerical/ experiment comparison)

For the situation of no impact, i.e., $l \sin \theta - gap > 0$, equation of motion is

$$ml^2\ddot{\theta} - mlA_0\Omega^2 \cos\theta \sin\Omega t + mgl\sin\theta = 0. \tag{2}$$

Once impact is modeled using continuous analysis, when the RIMD is impacting the cart ($l \sin \theta - gap \leqslant 0$), equation of motion will slightly change to

$$ml^2\ddot{\theta} - mlA_0\Omega^2 \cos\theta \sin\Omega t + mgl\sin\theta = F_i l; \ F_i = k_i\delta + c_i\dot{\delta}, \tag{3}$$

where the penetration δ and the velocity of penetration, $\dot{\delta}$ are described as

$$\delta = l\sin\theta - gap, \ \ \dot{\delta} = l\dot{\theta}\cos\theta. \tag{4}$$

It is important to emphasize that generalized coordinate θ (and therefore $\dot{\theta}$) is embarked on the cart. In order to compare with the experimental data, where the linear displacement is measured outside the cart using the laser sensor, the following transformations must take place:

$$x = l \sin \theta + A_0 \sin(\Omega t), \;\; \dot{x} = l \dot{\theta} \cos \theta + A_0 \Omega \cos(\Omega t) \tag{5}$$

As it will be shown on the numerical/ experiment comparison, although the system without impact presents some degree of damping, the mathematical modeling does not take it into consideration. For the case without impact, the test rig has a similar behavior to an oscillatory system with base excitation, having its resonance at 1.82 Hz. All numerical simulations were solved using the fourth order Runge-Kutta Method through the Matlab routine *ode45*.

For the case with impact, according to the Filippov theory [9], the mathematical modeling presented is a system described by differential equation with a discontinuous right-hand side, one condition for the case where no impact is present and another one for the impact case. Therefore, the state space $\dot{u} = f(u), u \in \mathbf{R}^n$ may be split into two subspaces Γ_- and Γ_+, separated by a hyper-surface Σ. Hyper-surface is defined by a scalar function $h(u)$. Consequently, the state u is in Σ when $h(u) = 0$. Hence, it is possible to define the subspaces Γ_- and Γ_+, as well as the hyper-surface Σ, using the sets:

$$\Gamma_- = \{u \in \mathbf{R}^n \mid h(u) < 0\}, \;\; \Sigma = \{u \in \mathbf{R}^n \mid h(u) = 0\}, \;\; \Gamma_+ = \{u \in \mathbf{R}^n \mid h(u) > 0\}. \tag{6}$$

Some physical systems need different interfaces in order to perform a correct description of the transitions. The impact force model used in the mathematical modeling is an example. Due to the nature of the impact model, the contact between the mass and the support occurs whenever the linear displacement becomes equal to contact gap. However, the mass loses contact with the support when the contact force (in this particular case, the moment) vanishes. In this case, two indicator functions are necessary in order to define the system subspaces (Savi et. al, 2007):

$$h_\alpha(\theta, \dot{\theta}) = l \sin \theta - gap, \;\; h_\beta(\theta, \dot{\theta}) = k_i \delta + c_i \dot{\delta}. \tag{7}$$

The mass is not in contact with the support if the state vector $u = (\theta, \dot{\theta}) \in \Gamma_-$, in other words:

$$\Gamma_- = \{u \in \mathbf{R}^2 \mid h_\alpha(\theta, \dot{\theta}) < 0 \text{ or } h_\beta(\theta, \dot{\theta}) < 0\}. \tag{8}$$

For the case when there is contact between the mass and the support:

$$\Gamma_+ = \{u \in \mathbf{R}^2 \mid h_\alpha(\theta, \dot{\theta}) > 0 \text{ and } h_\beta(\theta, \dot{\theta}) > 0\}. \tag{9}$$

The hyper-surface Σ consists of the conjunction of two surfaces Σ_α and Σ_β. The hyper-surface Σ_α defines the transition from Γ_- to Γ_+, i.e., when the mass initiates the contact with the support ($l \sin \theta - gap = 0$),

$$\Sigma_\alpha = \{u \in \mathbf{R}^2 \mid h_\alpha(\theta, \dot{\theta}) = 0 \text{ and } h_\beta(\theta, \dot{\theta}) \geqslant 0\}. \tag{10}$$

Surface Σ_β defines the transition from Γ_+ to Γ_- as the contact is lost when the impact force vanishes:

$$\Sigma_\beta = \{u \in \mathbf{R}^2 \mid h_\alpha(\theta, \dot{\theta}) \geqslant 0 \text{ and } h_\beta(\theta, \dot{\theta}) = 0\}. \tag{11}$$

Consequently, the state equation of this discontinuous system is written as follows:

$$\dot{u} = f(u, t) = \begin{cases} f_-(u, t), u \in \Gamma_- \\ \overline{co}\{f_-(u, t), f_+(u, t)\}, u \in \Sigma \\ f_+(u, t), u \in \Gamma_+ \end{cases} \tag{12}$$

where

$$f_-(u, t) = \begin{bmatrix} \dot{\theta} \\ \frac{A_0 \Omega^2}{l} \cos \theta \sin \Omega t - \frac{g}{l} \sin \theta \end{bmatrix}; u \in \Gamma_- \tag{13}$$

$$f_+(u,t) = \begin{bmatrix} \dot{\theta} \\ \frac{A_0\Omega^2}{l}\cos\theta\sin\Omega t - \frac{g}{l}\sin\theta + \frac{1}{ml}(k_i\delta + c_i\dot{\delta}) \end{bmatrix} \; ; \; u \in \Gamma_+ \tag{14}$$

$$\overline{co}\{f_-(u,t), f_+(u,t)\} = \begin{bmatrix} \dot{\theta} \\ \frac{A_0\Omega^2}{l}\cos\theta\sin\Omega t - \frac{g}{l}\sin\theta + \frac{1}{ml}(c_i\dot{\delta}) \end{bmatrix} ; in \; \Sigma_\alpha \tag{15}$$

$$\overline{co}\{f_-(u,t), f_+(u,t)\} = \begin{bmatrix} \dot{\theta} \\ \frac{A_0\Omega^2}{l}\cos\theta\sin\Omega t - \frac{g}{l}\sin\theta \end{bmatrix} ; in \; \Sigma_\beta \tag{16}$$

This approach allows one to deal with non-smooth systems employing a smoothened system. Leine (2000) also defines a finite region in order to consider transition subspaces. Therefore, a region of small relative displacement is defined as $|l\sin\theta - gap| < \eta$, where $\eta \ll 1$. The finite region is useful for numerical simulations since an exact value of zeros will not be computed. The thickness parameter of the narrow band η needs to be chosen according to the physical problem (Savi et. al, 2007).

The numerical/ experiment comparison starts with the chart of the non dimensional force (F_i/mg) in the frequency domain (Ω/ω), for each gap imposed on the test rig. These results are shown in Fig. 8. The methodology applied in order to identify the impact force is the same performed for the experimental data, where for each excitation frequency the maximum impact force is detected, regardless of the impact force behavior. As mentioned before, once impact force results do not change the peak value in each excitation frequency, except for the transitory bands, this routine seems to be quite effective, specially around the maximum impact force peaks.
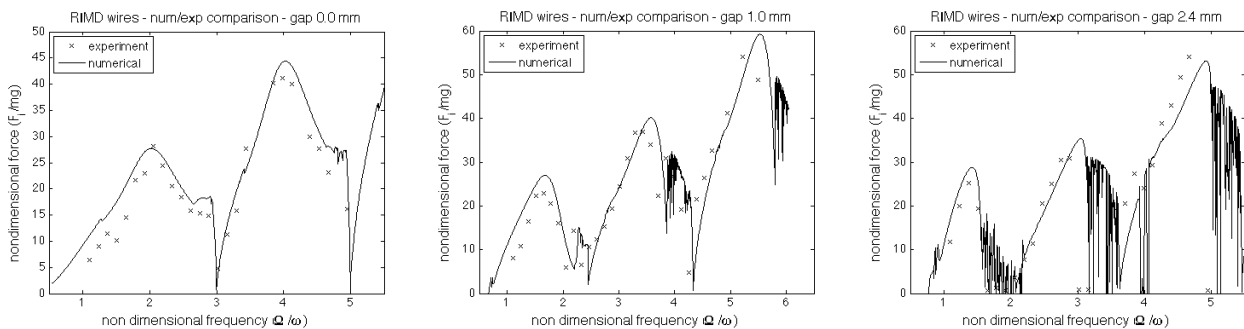
Figure 8. Numerical/ experiment comparison. Non dimensional force *versus* non dimensional frequency. *left*) Gap 0.0 mm. *center*) Gap 1.0 mm. *right*) Gap 2.4 mm.

The comparison shows a satisfactory agreement, specially concerning the impact resonance and the maximum impact force for the period-1 behavior, for each gap imposed. As it can be seen in Fig.s 9 and 10, where the numerical simulation is compared to the experimental data concerning the displacements over time, as well as the phase plane with the Poincaré maps.
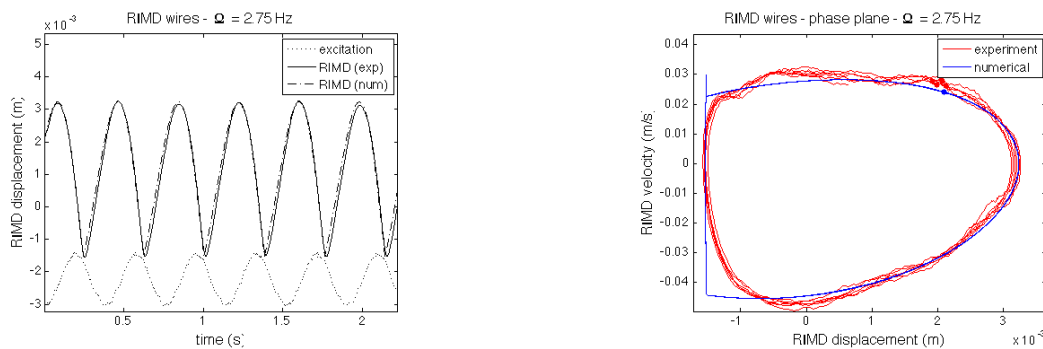
Figure 9. Period-1 behavior, gap 1.0 mm, non dimensional frequency 1.5: *left*) displacements; *right*) Phase plane (solid line) and Poincaré map (dots).
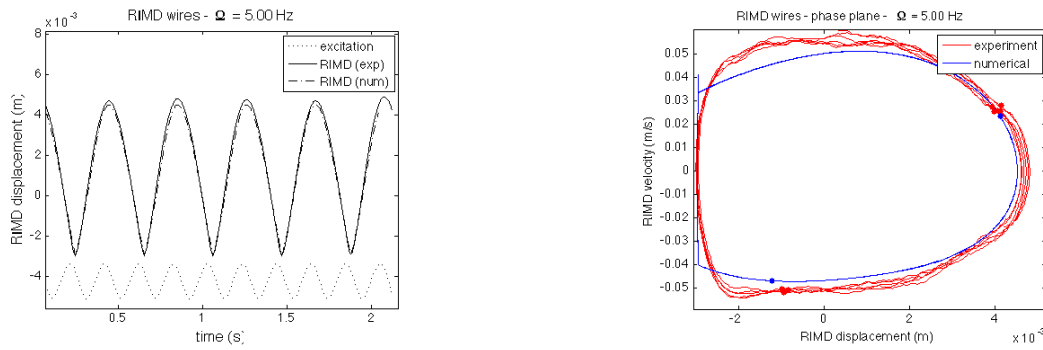
Figure 10. Period 0.5 behavior, gap 2.4 mm, non dimensional frequency 2.7: *left*) displacements; *right*) Phase plane (solid line) and Poincaré map (dots).

Although the impact force charts shown in Fig. 8 give some important information regarding the impact force amplitude and the frequency where the maxim impact is found (*impact resonance*), such charts provide no information about the characteristics of the impact force, neither details on the transition between frequency bands. To better understand the behavior of this dynamical systems, two nonlinear tools are further used. One is the Peterka map (Peterka, 1996), shown in Fig. 12, which provides information about the characteristic of the impact force as the gap is varied and the excitation frequency is swept. From this map it can be observed the areas where the two frequencies bands (detected during the experiment) take place, represented in red (period-1) and green (period 0.5). The second tool is the bifurcation diagram, where the transition band is observed in more detail, showing the conditions of picth-fork bifurcation (transition band for gap 0 mm) and chaos (gaps 1.0 mm and 2.4 mm).
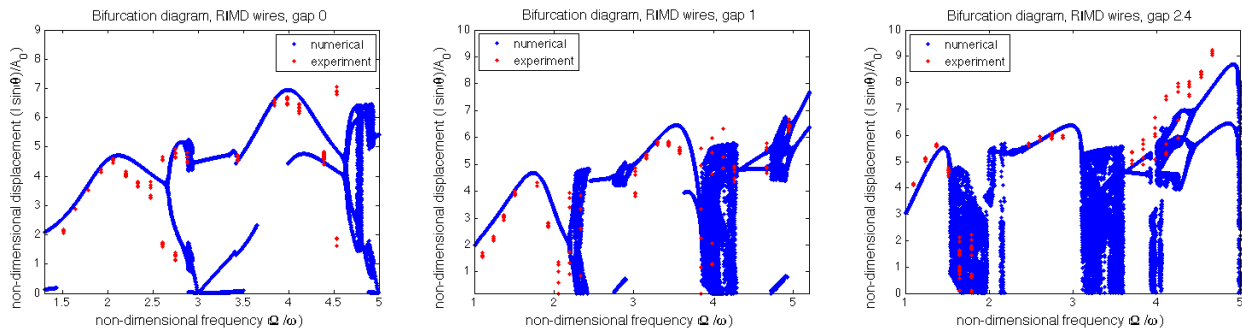
Figure 11. Numerical/ experiment comparison. Bifurcation diagrams, non-dimensional displacement, $l \sin \theta / A_0$. *left*) Gap 0.0 mm. *center*) Gap 1.0 mm. *right*) Gap 2.4 mm.

Finally, the presence of impact and the gap between the RIMD and the cart induces nonlinearity, and therefore nonlinear phenomena arise, specifically in the transition between frequency bands. One of these phenomena is the presence of basins of attraction for some gap conditions. In the Peterka map, Fig. 12, for a gap condition higher than 1.5, it exists an area between the period-1 (red) and period-0.5 (green) regions that are characterized by various impact conditions, which are extremely dependent on the system initial condition, as it could even be verified during the experiment, Fig. 12(*right*). In some conditions, where the system is excited by the AC motor, once some small amount of energy is inserted, the system will enter in a impact condition for some time and then return to the non-impact condition. However, for a similar condition, once some small amount of energy is inserted, the system will enter in a impact condition and remain in such state, as shown in Fig. 12(*right*).

4. CONCLUSIONS

The purpose of this work is the experimental and numerical investigation of the impact force behavior in a vibro-impact system, where such hammer is embarked on a cart that moves by a prescribed displacement. By changing the hammer characteristics and the impact gap it is possible to investigate the impact force behavior under different excitation frequencies. The motivation of this work is the oilwell drilling, where a new drilling technique, called ***Resonance Hammer Drilling***, is being developed, where the shock wave due to this hammer effect can be used to loose the system from a stick condition. It can also be of value if some brittle material is being cut. This present work is focused on the mathematical modeling of the experimental test rig presented in Aguiar and Weber (2008). In this case, the experimental data will be used to validate a mathematical model, where the system behavior is investigated in more detail, as well as a nonlinear analysis (bifurcation diagrams, Poincaré maps and Peterka map) is performed, showing the rich response of
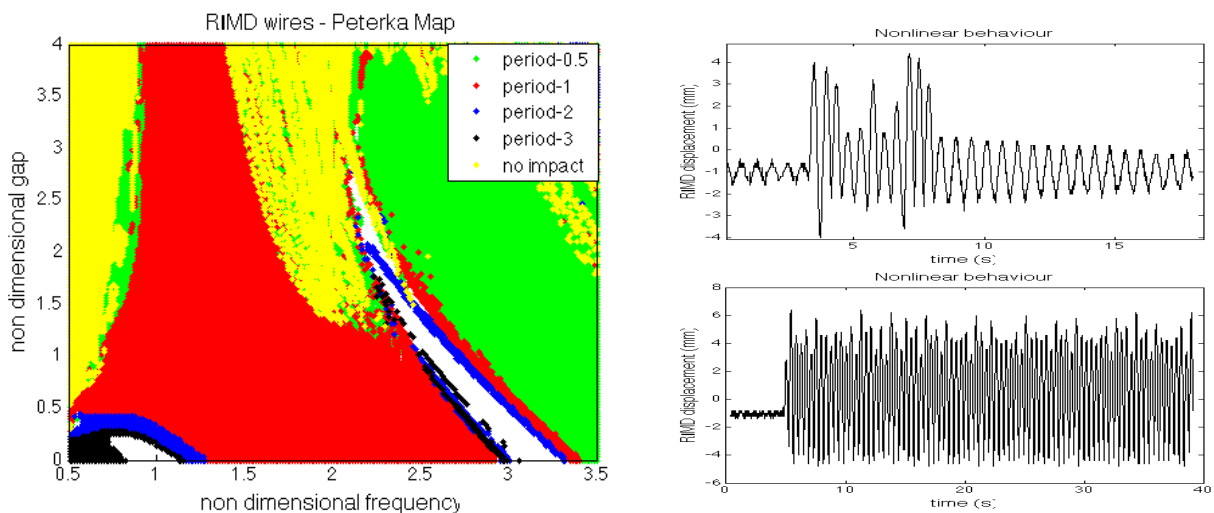
Figure 12. *left*) Peterka Map, non-dimensional gap (gap/A_0) *versus* non-dimensional frequency (Ω/ω). *right*) Nonlinear behavior (experimental). RIMD displacement over time: Condition of no impact/ energy inserted into the system/ system impacts but return to non-impact condition (up); b) Condition of no impact/ energy inserted into the system/ system impacts and remains in the impact condition (bottom).

the system, such as dynamical jumps, bifurcations and chaos. The numerical/ experiment comparison shows very good agreement.

5. ACKNOWLEDGEMENTS

6. REFERENCES

Aguiar, R.R. and Weber, H.I., 2009, "Development of a Vibroimpact Device for the Resonance Hammer Drilling", Proceedings of the XIII DINAME, Angra dos Reis, RJ, Brazil, 10 pgs, CD-ROM.

Aguiar, R.R and Weber, H.I., 2008, "On the Development of a Resonant Hammer", Proceedings of 9th MOVIC, September 15th-18th, Munich, Germany, 10 pgs, CD-ROM.

Detournay, E., 2004, "Enhanced Bit Performance through Controlled Drillstring Vibrations - Phase 3", Technical Report, Drilling Mechanics Group, CSIRO Petroleum, Kensington, WA, Australia.

Franca, L.F.P. and Weber, H.I., 2004, "Experimental and Numerical Study of a new Resonance Hammer Drilling Model with Drift", Chaos, Solitons and Fractals, Vol 21, pgs 789-801.

Gilardi, G. and Sharf, I., 2002, "Literature survey of contact dynamics modeling", Mechanism and Machine Theory, Vol 37, pgs 1213-1239.

Glocker, C. and Pfeiffer, F., 1996, "Multibody Dynamics with Unilateral Contacts", John Wiley and Sons.

Hunt, K.H. and Crossley, F.R.E., 1968, "Coefficient of Restitution Interpreted as Damping in Vibroimpact", Journal of Applied Mechanics - Transactions of the ASME, pgs 440-445.

Lankarani, H.M. and Nikravesh, P.E., 1994, "Continuous Contact Force Models for Impact Analysis in Multibody Systems", Nonlinear Dynamics, Vol 5, pgs 193-207.

Leine, R.I. and van Campen, D.H. and van de Vrande, B.L., 2000, "Bifurcations in nonlinear discontinuous systems", Nonlinear Dynamics, Vol. 23 (2), pgs 105-164.

Mattos, M.C. and Weber H.I., 1994, "Some Interesting Characteristics of a Simple Autonomous Impact System with Symmetric Clearance", ASME - Design Engineering Conference.

Peterka, F.,1996,"Bifurcations and Transition Phenomena in an Impact Oscillator", Chaos Solitons and Fractals, Vol.7, No.10, pgs 1635-1647.

Savi, M.A., Divenyi, S., Franca, L.F.P., Weber, H.I., 2007, "Numerical and Experimental Investigations of the Nonlinear Dynamics and Chaos in Non-smooth Systems", Journal of Sound and Vibration, Vol. 301, Iss. 1-2, pgs 59-73.

7. Responsibility notice

The authors are the only responsible for the printed material included in this paper